

All “roads” lead to rocksalt structure

Matthew Jankousky, Andrew Novick, and Vladan Stevanović*
Colorado School of Mines, Golden, CO 80401, USA

Helen Chen
Harvey Mudd College, Claremont, CA 91711, USA

(Dated: February 13, 2024)

Rocksalt is the most common crystal structure among binary compounds. Moreover, no long-lived, metastable polymorphs are observed in compounds with the rocksalt ground state. We investigate the absence of polymorphism and the dominance of the rocksalt structure via first-principles random structure sampling and transformation kinetics modeling of three rocksalt compounds: MgO, TaC, and PbTe. Random structure sampling reveals that for all three systems the rocksalt local minimum on the potential energy surface is far larger than any other, making it statistically the most significant structure. The kinetics modeling shows that virtually all other relevant structures, including most of the 457 known A_1B_1 prototypes, transform rapidly to rocksalt, making it the only option at ambient conditions. These results explain the absence of polymorphism in binary rocksalts, answer why rocksalt is the structure of choice for high-entropy ceramics and disordered ternary nitrides, and help understand/predict metastable states in crystalline solids more generally.

The rocksalt crystal structure dominates both binary compounds and entropy stabilized multi-component systems [1–7]. Within the A_1B_1 chemical space, which spans tetrahedrally bonded semiconductors (GaAs, SiC, GaN, ZnO, . . .), photovoltaic materials (CdTe), piezoelectrics (ZnO), thermoelectrics (PbTe), superconductors (NbN, FeSe) and other important functional materials, rocksalt is the most common crystal structure. There are 348 compounds with the rocksalt structure reported in the Inorganic Crystal Structure Database (ICSD) [8] out of 704 total A_1B_1 . Moreover, rocksalt is the ground state structure in the Materials Project database (MP) [9] for 238 of total 668 A_1B_1 compounds found in MP, as illustrated in Fig. 1. In contrast, the next most frequent A_1B_1 structure, zincblende, is the ground state for only 51 compounds. Rocksalt is also the most frequent structure among binaries as a whole. The next most common binary structures are fluorite (also s.g. #225) with 75 A_1B_2 compositions and the Uranium silicide-type structure (s.g. #221) with 66 A_1B_3 compositions. Regarding the entropy stabilized systems, disordered ternary nitrides often crystalize in the rocksalt structure [1–3]. High-entropy ceramics (oxides, nitrides, and carbides) with a 1:1 metal to nonmetal ratio always form in the rocksalt structure even when many parent compounds in an equimolar mixture are not rocksalts themselves [4–7].

While it is commonly associated with ionic compounds, the rocksalt ground state appears across the entire Van Arkel-Ketelaar bonding triangle [10] shown in Fig. 1, displaying that this structure is favorable in a variety of chemical environments. Arguments based on maximizing the packing factor for a given combination of ionic radii [11] or Phillips’ descriptor that chemically delineates which A_1B_1 systems will adopt a rocksalt structure

instead of a wurtzite structure [12] might help explain why rocksalt is the ground state structure. However, neither of these concepts is sufficient to predict or explain whether rocksalt compounds will have metastable polymorphs or not. For all the abundance and diversity of compounds with the rocksalt ground state, there are virtually no experimentally reported metastable polymorphs of A_1B_1 rocksalts in MP [9], ICSD [8] or available literature. The only reported cases are high pressure phases of the CsCl-type [84], NiAs-type [55], and KOH-type [31], and wurtzite in extremely thin films [16, 95] (see all compounds in Supplementary Table I). None of these 4 structures types represent long-lived, metastable states, as they all transform quickly to the rocksalt structure if the stabilizing pressure or strain is released (Supplementary Figure 5).

To elucidate the physical origins behind these observations, we investigate three specific systems with rocksalt ground state and distinct bonding characters: ionic MgO, largely metallic TaC, and covalent PbTe. Our analysis derives from the first-principles characterization of: (a) the sizes of the basins of attraction of different potential energy local minima (their “widths”), and (b) the transformation pathways and associated kinetic barriers for polymorphic transformations (“depths” of local minima). The “widths” of local minima correlate to experimental realizability, while the “depths” are connected to the lifetimes of polymorphs, and, as we will show, it is the interplay of these two features that explains the absence of polymorphism in rocksalt binary compounds and also its dominance in entropy-stabilized systems.

The “widths” of local minima are evaluated by the frequency of occurrence of a structure in the first-principles random structure sampling [18], which involves generating a large number of initial structures with random unit cell vectors and random atomic positions. Using density functional theory (DFT) [19], those random structures are relaxed to the closest local minimum on the potential

* vstevano@mines.edu

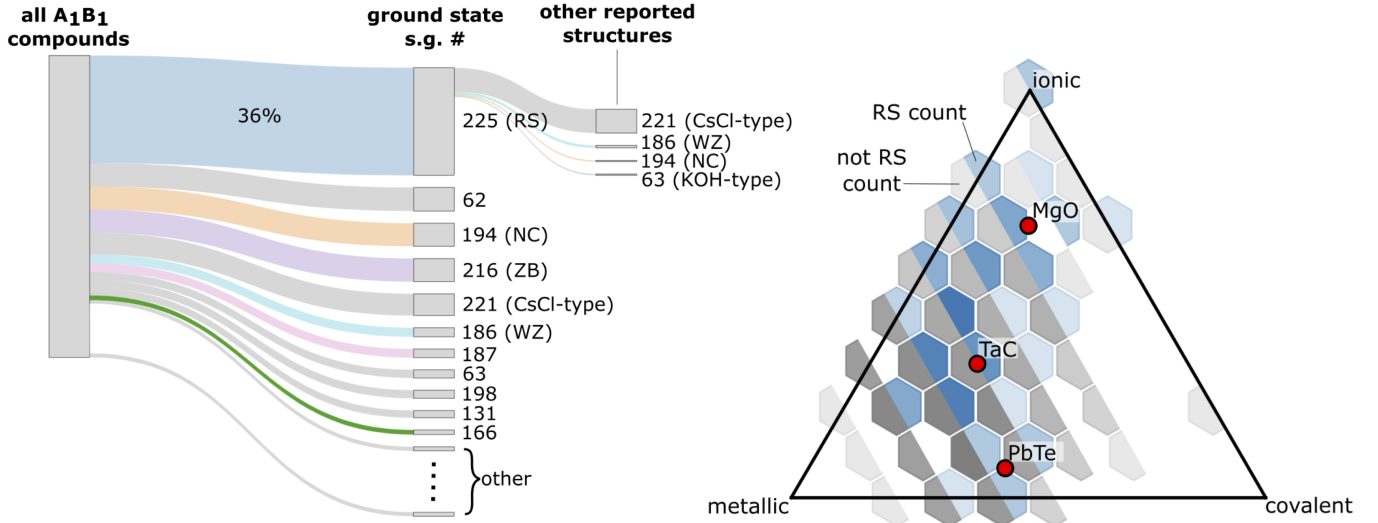


FIG. 1. (left panel) A sankey diagram showing the distribution of ground state structures (their space group numbers) among known A_1B_1 compounds. Other reported short-lived polymorphs of compounds with the rocksalt ground state are also shown. (right panel) The Van Arkel-Ketelaar bonding triangle populated with known A_1B_1 compounds. Darker hexes imply more compounds. Those with the rocksalt ground-state are highlighted in blue with the three compounds studied in this work depicted by red circles.

energy surface. The frequency of occurrence of a given structure after relaxations then measures the size of its attraction basin, that is, the total volume of configuration space occupied by that local minimum. Statistically, this frequency of occurrence represents the probability to fall into a given local minimum [20]. It has been shown that the experimentally realized metastable polymorphs are exclusively those with high frequencies of occurrence in the first-principles random structure sampling [2, 18, 20–22].

The “depths” of local minima are correspondingly measured by predicting mechanisms and associated energy barriers for diffusionless transformations between various structures. Mechanisms are identified by mapping crystal structures atom-to-atom in a way that minimizes the distance traveled by atoms along the pathway [23]. Energy barriers are estimated by computing the energy along the pathway without any relaxations. This provides an upper bound for the actual barrier. In cases where the upper limit is high, the minimal energy pathways are calculated with relaxations performed via solid-state nudged elastic band (SSNEB) method [24] using the mapping result as the starting point.

Note that this procedure assumes concerted motion of atoms during the phase transformation, and as such does not include interface effects associated with nucleation and growth. Because of this, when evaluating if a phase transition is rapid or sluggish, we follow a broadly adopted semi-quantitative distinction [25]. In short, barriers close to 100 meV/atom or lower would be classified as allowing rapid phase transformations, while those with barriers much above this value would be classified as characteristic of sluggish transformations [26]. The

transformation mechanisms and energy profiles from this work are collected into a database of pathways that is provided in Supplementary Information.

Exploration of the relevant crystal phases of the three rocksalt compounds from the first-principles random structure sampling shows that their potential energy surfaces share many of the same features, as summarized in Fig. 2(a). For MgO, the rocksalt structure is found for more than half of the random structures, or 1061 times out of 2000 total random structures needed to achieve converged results. The frequency of the next most frequent structure is lower by a factor of ~ 20 . For TaC, rocksalt occurs less frequently, making up about 4 % of the relaxed random structures, but it is more frequent than the next one by a factor of ~ 5 . For PbTe, the rock-salt structure also occurs ~ 4 % of the time (80 out of 2000), and it is about 40 times more frequent than the next one.

The majority of other structures found in the random sampling have no symmetry at all (s.g. #1). They represent a “sea” of local minima, the number of which increases exponentially with the system size [27]. Extrapolation to an infinite number of initial random structures would return negligible probabilities of occurrence for all of them. There are also more symmetric structures that exhibit stable frequencies of occurrence as a function of the number of random structures. These occur much less frequently than rocksalt and are consequently less likely to be realized. They share some common structural features with the rocksalt structure. Most are built from different arrangements of 6-fold coordination polyhedra including face-sharing and/or edge-sharing octahedra and trigonal prisms. Structures consisting of these

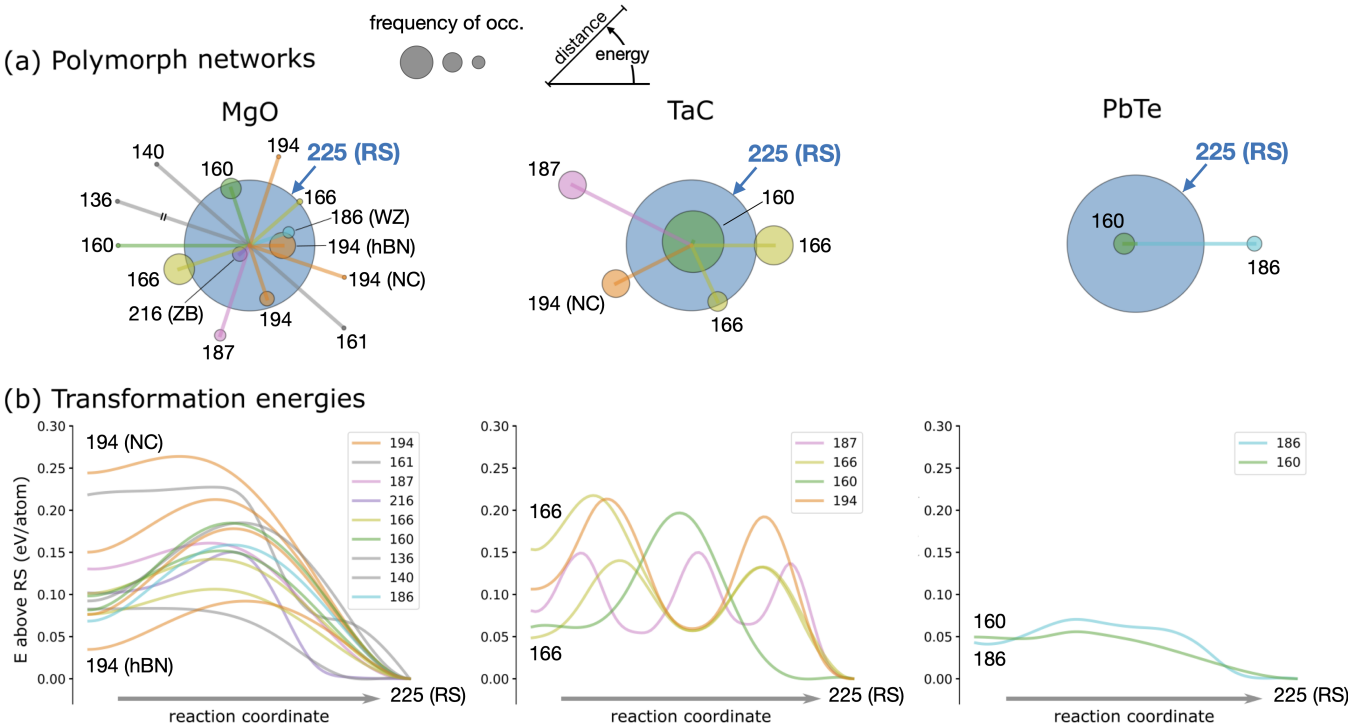


FIG. 2. (a) Networks representing the high-symmetry polymorphs identified by random sampling in MgO, TaC, and PbTe. The rocksalt structure is the central node of each network. All other structures are labeled according to their space group number. The size of each node represents the frequency of occurrence of a structure in the random sample. Note that a fixed size is used to represent the width of the rocksalt local minimum, and other points are scaled relative to this size. Structures are arranged so that the energy increases with the polar angle and the distance of each node from the rocksalt center is proportional to the distance travelled by the atoms during phase transformation of that structure to rocksalt. (b) Calculated (SSNEB) energy profiles along the transformation from the high-symmetry structures identified in the random sampling to the rocksalt structure.

motifs include those with s.g. # 160, 166, 187, and 194 in MgO, s.g. # 160, 166, 187, and 194 in TaC, and s.g. # 160 and 186 in PbTe. MgO is the only chemistry which exhibits symmetric structures that do not all fall into the above categories. These other structures include the tetrahedrally coordinated zincblende (ZB, s.g. #216) and wurtzite (WZ, s.g. #186) structures, a hexagonal boron nitride (hBN, s.g. # 194), and a buckled hBN (s.g. #136) structure, as well as a structure consisting of MgO_6 octahedra and MgO_5 trigonal bipyramids with long channels running in the c-direction (s.g. # 140).

We now turn to the question of the lifetimes of higher energy, symmetric structures found by the random sampling. If any of them could potentially be realized in spite of their narrow local minima it is important to ask whether they would be long-lived (metastable). Interestingly, for all three chemistries, structure mapping combined with SSNEB calculations finds that all symmetric structures identified by the random sampling have low energy barriers ($\lesssim 100$ meV/atom) for transformations to the rocksalt ground state. The results are summarized in Fig. 2(b) and the mechanisms are provided in Supplementary Information as part of the pathways database. For the 6-fold coordinated structures, conversion to rock-

salt generally involves a slipping process that transforms trigonal prisms to octahedra and/or changes the orientation of octahedra from face- to edge-sharing. For the structures with MgO_x polyhedra with $x < 6$, mechanisms also include an increase in coordination from 4 or 5 to 6.

Among structures found in random sampling, the highest barrier for transformations to rocksalt is 127 meV/atom. This is for the TaC structures with s.g. #194 and 160. Their predicted transformation mechanisms have the same rate limiting steps because the structure with s.g. #160 is an intermediate local minimum along the pathway from s.g. #194 to the rocksalt structure. As a result of the relatively low energy barriers for transformation to rocksalt, all symmetric structures from the random sampling are expected to have short lifetimes at ambient conditions.

These results explain the lack of metastable polymorphs in binary rocksalts. They imply that for all three studied chemistries the local minimum corresponding to the rocksalt structure is 5 to 40 times larger than any other and is hence, statistically much more significant. Additionally, all other, statistically non-negligible local minima would be short-lived as the kinetic barriers are not high enough to ensure kinetic trapping.

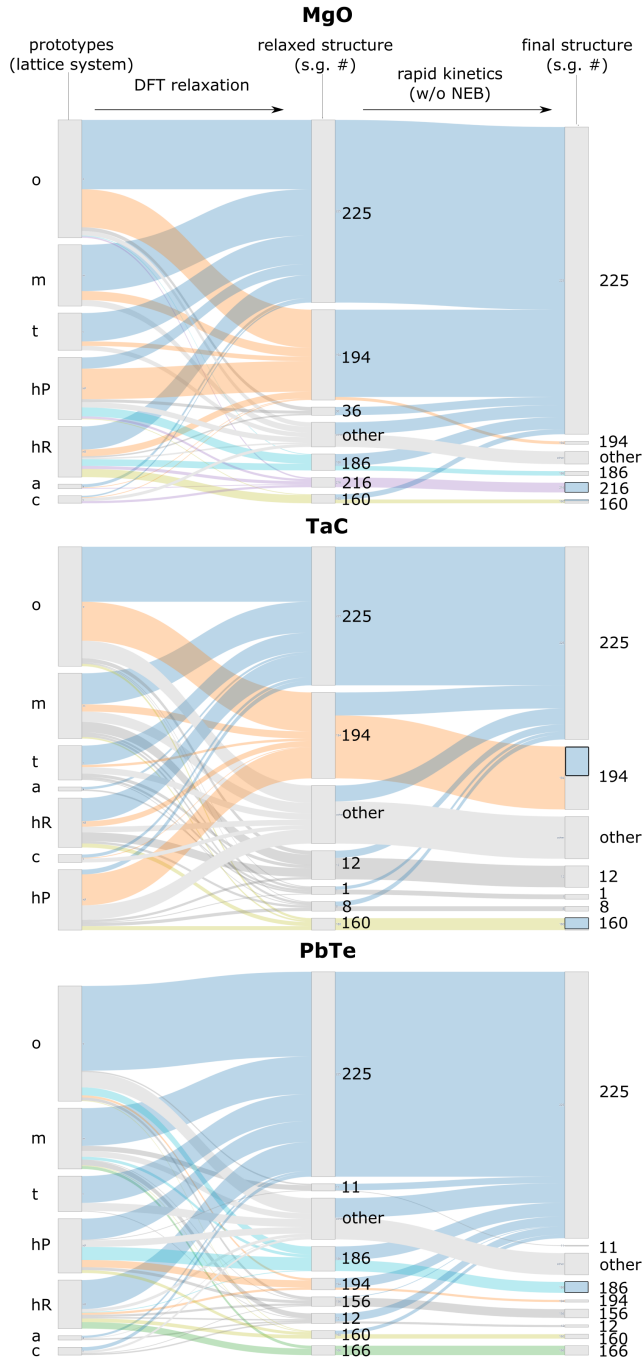


FIG. 3. Sankey diagrams showing the kinetic flow of 457 prototype structures found in the ICSD spanning the A_1B_1 chemical space for each of MgO, TaC, and PbTe. The bars on the left represent the distribution of the A_1B_1 prototypes across 7 crystal systems. Bars in the center display the distribution of space groups that these prototypes relax into. Structures which link to the s.g. #225 bar at the right end have kinetic barriers for transformation to rocksalt less than 150 meV/atom.

What about other structures? It is also interesting to investigate whether these conclusions hold for other

structures not found by the random sampling. According to ICSD, A_1B_1 compounds crystallize in 457 different structures types (see Methods). To test which of these would constitute local minima for the three studied chemistries and how shallow they might be, we substituted the MgO, PbTe and TaC chemistries in all A_1B_1 prototype structures from ICSD and relaxed them using DFT. For the resulting relaxed structures, we estimated their kinetics for transformation to the rocksalt using our structure mapping method. The results are summarized in Fig. 3.

For MgO, TaC, and PbTe, respectively, 245, 174, and 283 of the 457 prototypes relax spontaneously to rocksalt structure implying zero or nearly zero barriers. For the remaining structures, pathways that have static energy profiles with maximum energy below 150 meV/atom are considered characteristic of a rapid transformation to rocksalt. We use 150 meV/atom because our structure mapping result is an estimate of the upper bound for the barriers. The ssNEB calculations will, in most cases, relax to a minimal energy pathway with a lower barrier. Adding this criterion, a total of 412, 251, and 369 of the 457 prototypes are estimated to transform quickly to the rocksalt structure in MgO, TaC, and PbTe.

These are relatively large fractions of common A_1B_1 structures, in particular for MgO and PbTe. TaC seems a little different, but it is important to note that the 108 prototypes that relax directly to structures with s.g. #194 include 38 that end in the nickelene (NC) structure type, which has a low barrier for transformation into rocksalt according to our SSNEB calculations (see Fig. 2(b)). These are marked by the blue rectangle in Fig. 3. The same is true for s.g. #160 in TaC, s.g. #216 for MgO, and s.g. #186 for PbTe. In summary we can say that 291 out of 457 prototypes (64%) transform quickly to rocksalt in TaC. While not all prototypes transform rapidly into rocksalt, those that do not are, according to the random structure sampling, statistically insignificant and based on the collected evidence should be very hard if not impossible to realize.

What if rocksalt is not the ground state? For many A_1B_1 compounds the ground state is not rocksalt, but it does appear as either a high pressure phase or a phase that can be epitaxially stabilized. Our results are relevant for these situations too, as only the structures that have energies in between the ground state and the rocksalt structure are plausible candidates for the metastable states. Most of those with energies above rocksalt will tend to transform rapidly into the rocksalt which will then likely transform quickly into the ground state, making them short-lived. In this way, the energy of the rocksalt structure then represents an energy limit for the likely metastable states. This is of course true for the larger fraction of prototypes that do transform rapidly. To what extent the rocksalt structure a limit of metastability for the A_1B_1 chemistry can be seen in Fig. 4.

We find that for most A_1B_1 compositions which have rocksalt as a high energy structure according to MP [9],

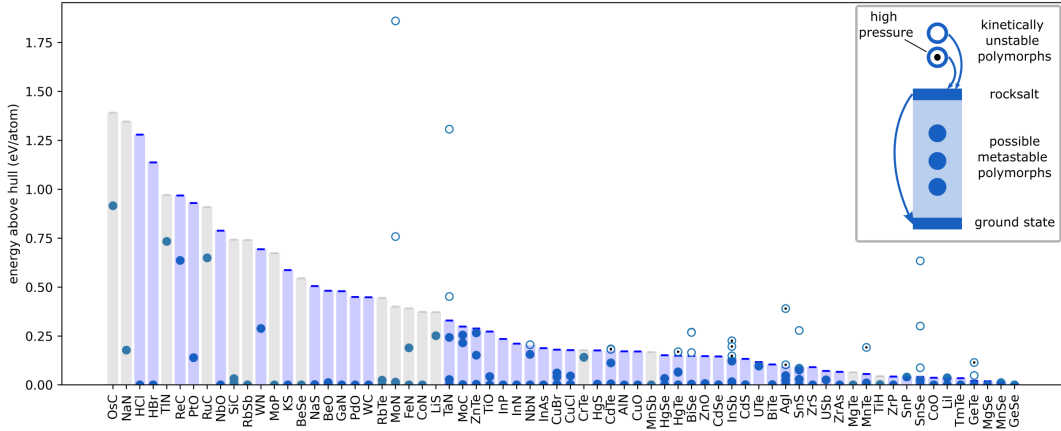


FIG. 4. Energies of reported polymorphs for A_1B_1 chemistries where rocksalt is reported as a high energy polymorph. Bars represent the energy of the rocksalt relative to the convex hull, experimentally realized rocksalts are blue, while theoretical ones are grey. Other experimentally realized polymorphs with energy below rocksalt are filled blue dots, while polymorphs with energy above rocksalt are open blue circles, and high pressure structures with energy above rocksalt are additionally marked with a black dot. The only reported polymorphs with energy above rocksalt are those in the exception categories specified in the text.

other experimentally reported polymorphs have their total energy equal or below the rocksalt structure. The only exceptions to this trend (open circles) are (i) high pressure phases that transform quickly to rocksalt and are not metastable (open circles with black dot), (ii) misfit layered compounds, which are formed by thin layers of two different compounds (see SI) [28], and (iii) instances with misassigned structure type. This is all evident if we take SiC as an example. It has a relatively corrugated potential energy surface with polytypes in the family of zincblende, wurtzite, and a tetrahedrally coordinated rhombohedral structure all forming as metastable polymorphs and all having energies below rocksalt as confirmed by the random structure sampling [22]. A polymorph network and a Sankey diagram for SiC are provided in Supplementary Figures 7 and 8.

Metastable polymorph discovery beyond A_1B_1 . The realization that in A_1B_1 chemistries most structures with energies above rocksalt will transform quickly to rocksalt and then to the respective ground-state may offer a general insight for the discovery of metastable polymorphs in other compositions. Stoichiometries other than A_1B_1 may behave the same way provided that a structure playing the role of the rocksalt exists. Some evidence for the A_1B_2 chemistry can be found in the literature. Namely, the fluorite structure (also s.g. # 225) is the most commonly observed A_1B_2 structure and it is well documented (Ref. [23] and the references therein) that the transformations from the highest-pressure fluorite structure to other observed lower pressure phases of SnO_2 including the ground-state rutile are all rapid, indicating fluorite may play a role similar to that of rocksalt in A_1B_1 (See Supplementary Information Table VII). Indeed, A_1B_2 compositions with the fluorite ground state have only cotunnite as a possible metastable polymorph, and there

are reports of it also transforming rapidly into fluorite [157]. Additionally, all known polymorphs of SiO_2 have their total energies below that of fluorite (see Supplementary Information Table VIII).

Relevance to high entropy systems. The arguments connecting “widths” of the local minima on the potential energy surface to experimental realizability apply also to atomic disorder and entropy stabilized systems. An intriguing fact is that virtually all equimolar mixtures of A_1B_1 binaries are stabilized in the rocksalt structure even when a number of components are not rocksalts themselves. The exceptions are high-entropy borides, which form in a hexagonal structure with layers of edge sharing octahedra which share faces with the octahedra in adjacent layers, likely due to the tendency of boron to form rings. While simplistic entropy arguments based on counting configurations of atoms on a given lattice offer an explanation for the formation of the mixture as opposed to the phase separation [6, 7], there is no explanation as to why the rocksalt structure is observed and not some other. Namely, contributions to configurational entropy from different arrangements of atoms are the same irrespective of the type of the crystal structure.

Based on the previous discussion we can say that in a given mixture each individual arrangement of atoms having the rocksalt structure as the underlying (parent) structure could be considered a relatively “wide” local minimum. The width of the rocksalt local minimum is also relevant for mixtures as it allows relatively large distortions away from the ideal rocksalt structure while still remaining inside the rocksalt basin of attraction. Then all those arrangements of atoms (cations and/or anions) will collectively form a very wide “valley” on the potential energy surface corresponding to the disordered rock-salt phase. Because of all this it could be hypothesized

that rocksalt will remain statistically the most significant structure even when a large fraction of components are not rocksalts themselves.

We put this hypothesis to test by performing the random structure sampling for a hypothetical $(\text{MgO})(\text{ZnO})(\text{CuO})$ mixture. Out of the three oxides, only MgO crystallizes in the rocksalt structure, while both ZnO and CuO strongly favor 4-fold coordination in their ground states. Random structure sampling results show disordered rocksalt as the highest occurring structure-type with different atomic configurations spanning a relatively narrow energy range as evidenced by the thermodynamic density of states (see Fig. 9 in Supplementary Information). Hence, in spite of only 1/3 of cations favoring rocksalt structure, it remains statistically the most significant crystal structure of all.

Another interesting example supporting our discussion is ZnZrN_2 ternary nitride, which is found in thin-film synthesis to always form in the disordered rocksalt structure in spite of having a well-defined non-rocksalt (layered) ground state [2]. The case of ZnZrN_2 is particularly interesting as many other structure-types are calculated to have lower energies than the cation-disordered rocksalt phase [2]. The random structure sampling reported in Ref. [2] once again shows that the cumulative frequency of occurrence of the collection of the disordered rocksalt configurations is ~ 100 times higher than the ground state, which appears as a very narrow local minimum in comparison to the rocksalt. Hence, our findings are also consistent with the difficult experimental realization of the ZnZrN_2 in its ordered ground state structure and the realization of the disordered rocksalt instead, as a consequence of the high configurational entropy of the disordered rocksalt originating from the large fraction of the configurational space that can be assigned to the rocksalt structure.

I. CONCLUSION

In this paper we examine the lack of metastable polymorphs among compounds with A_1B_1 stoichiometry and the rocksalt ground state. Using first-principles random structure sampling and transformation kinetics modeling we show that a combination of probabilistic and kinetic factors is responsible for the lack of polymorphism in this important group of materials. Namely, we demonstrate using ionic MgO , metallic TaC and covalent PbTe as case studies, that metastable polymorphs are not found among A_1B_1 rocksalts because (a) the rocksalt structure represents a very large local minimum on the potential energy surface in comparison to other structures, which makes it statistically much more significant than any other, and (b) that virtually all relevant crystal structures including those found by the random structure sampling as well as the majority of the A_1B_1 structure prototypes transform rapidly to the rocksalt structure. Moreover, the minority of the prototypes that do not

transform rapidly all represent a very narrow local minima according to the random sampling, and, are therefore statistically insignificant. In other words, while they may be candidate metastable structures their experimental realization is predicted to be very difficult if not entirely unlikely. In addition, we showed that same arguments can be extended to explain observed polymorphs in A_1B_1 compounds that do not have rocksalt ground state, and possibly also in other chemistries. Probabilistic factors (“width” of local minima) are also found to be responsible for the realization of the disordered rocksalt structure in high-entropy ceramics and disordered ternary nitrides. Lastly, all transformation pathways from A_1B_1 prototypes to the rocksalt structure are collected in a database provided in Supplementary Information.

ACKNOWLEDGMENTS

This work is supported by the National Science Foundation, Grant No. DMR-1945010 and was performed using computational resources provided by Colorado School of Mines and using services provided by the PATH Facility, which is supported by the National Science Foundation award #1836650. The support of the NSF-funded REU program at Colorado School of Mines, Grant No. DMR-1950924, is also acknowledged.

II. METHODS

A. First-principles random structure sampling

We evaluate which local minima are statistically relevant via the first-principles random structure sampling [18]. In this sampling, lattice vectors with a random choice of parameters $a, b, c, \alpha, \beta, \gamma$ are generated. A given number of atoms are then distributed over two interpenetrating grids of points, one for cations and the other for anions, to promote cation-anion coordination. Grids are constructed by discretizing a family of planes defined by the reciprocal lattice vector $\mathbf{G} = n_1\mathbf{g}_1 + n_2\mathbf{g}_2 + n_3\mathbf{g}_3$ with a random choice of n_1, n_2, n_3 . Cations and anions are distributed along the minima and maxima of a plane wave defined by $\cos(\mathbf{G}\mathbf{r})$, respectively. To prevent atoms from being placed too close to one another, a probability distribution is constructed of Gaussians centered at the location of each atom, and new atoms are placed in regions where the sum of Gaussians is low. In this work supercells with 24 atoms are generated, and the number of random structures is chosen based on the convergence of the appearance of different structures within the samples. Plots demonstrating this convergence can be found in the Supplementary Information Figure 10. This results in approximately 2000 structures for MgO , 1000 structures for TaC , and 2000 structures for PbTe . Once a structure is generated, it is then relaxed using DFT

to its closest local minimum on the potential energy surface. After relaxations are finished the relaxed structures are then grouped into classes of equivalent structures if (a) their space group assignments are the same, (b) their energies are within 10 meV/atom, (c) their volumes are within 5 %, and (d) and the coordination numbers of atoms up to 3rd coordination shell are the same.

B. Density functional theory relaxations

Relaxations of the random structures include all degrees of freedom (cell shape, volume, atomic positions) and are performed using the conjugate gradient algorithm such that each structure relaxes to its closest local minimum on the potential energy surface with high probability. Forces for the conjugate gradient algorithm are evaluated with density functional theory [19] using the Vienna *ab initio* Simulation Package (VASP) [30]. The relaxtions are performed with the generalized gradient approximation, specifically, the Perdew-Burke-Ernzerhof exchange-correlation functional [31]. Electronic degrees of freedom are described within the projector-augmented wave (PAW) formalism [32]. The plane-wave cutoff used in all calculations is 540 eV, and the Monkhorst-Pack \mathbf{k} -point grids [33] are automatically generated with a length parameter of 20 to achieve uniform subdivisions along the reciprocal lattice vectors in all structures. The electronic structure is considered converged when the change in total energy between steps of the Davidson algorithm is less than 10^{-6} eV. The ionic positions are considered converged when the change in energy between steps of the conjugate gradient algorithm for ionic positions is less than 10^{-5} eV. For numerical reasons cell shape and volume relaxations are restarted at least 3 times followed by a self-consistent run. All structures with final pressures above 3 kbar calculated in the final, self-consistent run are re-relaxed until final pressures are all below 3 kbar.

C. Barrier approximation

Once high symmetry structures are identified via random sampling, their barrier for a concerted transformation to the rocksalt structure is approximated. Optimal atom-to-atom mapping is performed between each relevant local minimum and the rocksalt structure as in [23]. In this mapping, different representations of the unit cell of each structure are compared to identify those combinations with maximum volumetric overlap, to minimize the distortion of the unit cell along the pathway. For cells with maximum volumetric overlap, atoms are matched between the two structures by way of the Munkres algorithm [34], an iterative solution of the assignment problem. Iterating over unit cell combinations with the Munkres algorithm returns mappings with minimized distance traveled by the atoms during the

concerted transformation. For each mapping, the first shell coordination is computed for ten images along the transformation. We find that mappings with monotonic changes in coordination have smaller barriers, so these are used as starting points where possible. If there is no path with monotonic change in coordination, the path chosen is that with the smallest change in coordination, if multiple paths have the same change in coordination along the path, the path with the shortest distance is used.

An upper bound for the energy barrier of this transformation can be computed by calculating the energy of each image along the path. Energy is calculated using the same parameters as the relaxations, but the structures along the path are not allowed to relax. The energies are calculated for structures identified from the random sample, if the barrier ($E_{max,path} - E_{polymorph}$) is found to be greater than 100 meV/atom, we perform solid state nudged elastic band (SSNEB) calculations to find the minimum energy pathway near the pathway predicted as above [24]. The SSNEB calculations are considered converged when the force perpendicular to the tangent along the path is less than 0.1 eV/Angstrom. Initial calculations use 9 intermediate images, if these calculations exhibit intermediate local minima, the local minima are relaxed, and a new SS-NEB calculation is performed between the local minima along the pathway in order to converge each step along the path.

D. Database of transformation mechanisms

To determine if prototypical A_1B_1 structures are likely to transform quickly to the rocksalt structure and to begin the population of a database of NEB starting points, we used the AFLOW Xtalfinder [35] to classify each A_1B_1 structure in the ICSD as belonging to an AFLOW prototype [36]. For some prototypes, all atoms occupy fixed Wyckoff positions and the only variable parameter is the lattice constant. For these cases, only a single representative of that prototype is needed in each chemistry. For those where there exist structures in the ICSD with different lattice constant ratios and variable wyckoff positions such that atom positions vary between members of the same prototype, structures are classified as equivalent using the AFLOW Xtalfinder [35], such that every distinct structure found in the ICSD for a given prototype is represented. If swapping A and B sites leads to different coordination of A and/or B atoms, the swapped structure is also considered.

For each prototypical structure identified in this way, the A and B sites are populated with the elements of the three example compounds. The lattice constant is then scaled such that the average bond length between A and B atoms is equal to the bond length found in the rocksalt structure for each chemistry. Atoms are then perturbed by 0.3 Angstroms, and the perturbed structures are relaxed as described in the “Density Functional

Theory Calculations” section.

The resulting structures are grouped according to their AFLOW prototype labels, and the resulting distribution of space groups is the second column of nodes in Fig. 3. An atom-to-atom map is generated from each unique structure to the rocksalt structure, as in the “Barrier approximation” section. Only the static barriers are

computed for these structures. Those structures with a kinetic barrier to the rocksalt structure of 150 meV or less are considered to have rapid kinetics, and are added to the rocksalt node in the third column of Fig. 3. The structures with static barriers of greater than 150 meV/atom are grouped by their space group in third column of Fig. 3.

[1] W. Sun, C. J. Bartel, E. Arca, S. R. Bauers, B. Matthews, B. O. nanos, B.-R. Chen, M. F. Toney, L. T. Schelhas, W. Tumas, J. Tate, A. Zakutayev, S. Lany, A. M. Holder, and G. Ceder, *Nature Materials* **18**, 732 (2019).

[2] R. Woods-Robinson, V. Stevanović, S. Lany, K. N. Heinzelman, M. K. Horton, K. A. Persson, and A. Zakutayev, *Phys. Rev. Mater.* **6**, 043804 (2022).

[3] S. R. Bauers, A. Holder, W. Sun, C. L. Melamed, R. Woods-Robinson, J. Mangum, J. Perkins, W. Tumas, B. Gorman, A. Tamboli, G. Ceder, S. Lany, and A. Zakutayev, *PNAS* **116**, 14829 (2019).

[4] C. Osse, C. Toher, and S. Curtarolo, *Nature Review Materials* **5**, 295 (2020).

[5] C. M. Rost, E. Sachet, T. Borman, A. Moballegh, E. C. Dickey, D. Hou, J. L. Jones, S. Curtarolo, and J.-P. Maria, *Nature Communications* **6**, 8485 (2015).

[6] P. Sarker, T. Harrington, C. Toher, C. Osse, M. Samiee, J.-P. Maria, D. W. Brenner, K. S. Vecchio, and S. Curtarolo, *Nature Communications* **9**, 4980 (2018).

[7] S. J. McCormack and A. Navrotsky, *Acta Materialia* **202**, 1 (2021).

[8] A. Belsky, M. Hellenbrandt, V. L. Karen, and P. Luksch, *Acta Crystallogr., Sect. B* **58**, 364 (2002).

[9] A. Jain, S. P. Ong, G. Hautier, W. Chen, W. D. Richards, S. Dacek, S. Cholia, D. Gunter, D. Skinner, G. Ceder, and K. A. Persson, *APL Materials* **1**, 011002 (2013).

[10] L. C. Allen, J. F. Capitani, G. A. Kolks, and G. D. Sproul, *Journal of Molecular Structure* **300**, 647 (1993).

[11] J. K. Kummerfeld, T. S. Hudson, and P. Harrowell, *The Journal of Physical Chemistry B Letters* **112**, 10773 (2008).

[12] J. C. Phillips, *Rev. Mod. Phys.* **42**, 317 (1970).

[84] S. Abrahams and J. Bernstein, *Acta Crystallographica* (1,1948-23,1967) **18**, 926 (1965).

[55] S. Weir, Y. Vohra, and A. Ruoff, *Physical Review, Serie 3. B - Condensed Matter (18,1978-)* **33**, 4221 (1986).

[31] S. Hull and D. Keen, *Physical Review, Serie 3. B - Condensed Matter (18,1978-)* **59**, 750 (1999).

[16] C. Martínez-Boubeta, A. S. Botana, V. Pardo, D. Baldomir, A. Antony, J. Bertomeu, J. M. Rebled, L. López-Conesa, S. Estradé, and F. Peiró, *Physical Review B* **86**, 041407 (2012).

[95] N. K. Min, K. Yong-Il, J. Younghun, L. S. Mi, K. B. G., C. Ran, C. Sang-Il, S. Hyunjoon, and P. J. T., *Journal of the American Chemical Society* **134**, 8392 (2012).

[18] V. Stevanović, *Phys. Rev. Lett.* **116**, 075503 (2016).

[19] P. Hohenberg and W. Kohn, *Phys. Rev.* **136**, B864 (1964).

[20] E. B. Jones and V. Stevanović, *Phys. Rev. B* **96**, 10.1103/PhysRevB.96.184101 (2017).

[21] C. M. Caskey, A. Holder, S. Shulda, S. Christensen, D. Diercks, C. Schwartz, D. Biagioni, D. Nordlund, A. Kukliansky, A. Natan, et al., *J. Chem. Phys.* **144**, 144201.

[22] M. Jankousky, E. M. Garrity, and V. Stevanović, *Physical Review Materials* **7**, 053606 (2023).

[23] V. Stevanović, R. Trottier, C. Musgrave, F. Therrien, A. Holder, and P. Graf, *Phys. Rev. Mater.* **2**, 10.1103/PhysRevMaterials.2.033802 (2018).

[24] D. Sheppard, P. Xiao, W. Chemelewski, D. D. Johnson, and G. Henkelman, *J. Chem. Phys.* **136**, 074103 (2012).

[25] D. R. Trinkle, R. G. Hennig, S. Srinivasan, D. M. Hatch, D. Jones, H. T. Stokes, R. C. Albers, and J. W. Wilkins, *Physical Review Letters* **91**, 025701 (2003).

[26] For example, barrier for the concerted diamond-to-graphite transformation is estimated to be \sim 300 meV/atom.

[27] F. H. Stillinger, *Phys. Rev. E* **59**, 48 (1999).

[28] G. Wiegers, *Progress in Solid State Chemistry* **24**, 1 (1996).

[157] E. Morris, T. Groy, and K. Leinenweber, *Journal of Physics and Chemistry of Solids* **62**, 1117 (2001).

[30] G. Kresse and J. Hafner, *Phys. Rev. B* **47**, 10.1103/PhysRevB.47.558 (1993).

[31] J. P. Perdew, K. Burke, and M. Ernzerhof, *Phys. Rev. Lett.* **77**, 10.1103/PhysRevLett.77.3865 (1996).

[32] G. Kresse and D. Joubert, *Phys. Rev. B* **59**, 10.1103/PhysRevB.59.1758 (1999).

[33] H. J. Monkhorst and J. D. Pack, *Phys. Rev. B* **13**, 5188 (1976).

[34] H. W. Kuhn, *Naval research logistics quarterly* **2**, 83 (1955).

[35] D. Hicks, C. Toher, D. C. Ford, F. Rose, C. D. Santo, O. Levy, M. J. Mehl, and S. Curtarolo, *npj Comput. Mater.* **7**, 30 (2021).

[36] M. J. Mehl, D. Hicks, C. Toher, O. Levy, R. M. Hanson, G. Hart, and S. Curtarolo, *Computational Materials Science* **136**, S1 (2017).

compound	polymorph	space groups	structure types	realization condition	citations
INa	141			mislabeled	[1, 2]
PrSb	123	CsCl		high pressure	[3, 4]
CeSb	123	CsCl		high pressure	[5, 6]
PuSb	123, 221	CsCl		high pressure	[7, 8]
IRb	221	CsCl		high pressure	[9, 10]
LaAs	123	CsCl		high pressure	[11, 12]
PbTe	221, 62	CsCl, Distorted RS		high pressure	[13–16]
KCl	221	CsCl		high pressure	[10, 17]
TlI	221, 63	CsCl, Distorted RS		high pressure	[18–20]
CTl	99, 221	CsCl		high pressure	[21–23]
MgO	186, 187	Wurtzite		thin film	[24–26]
CaTe	221	CsCl		high pressure	[27, 28]
TlCl	221, 63	CsCl, Distorted RS		high pressure	[19, 29, 30]
ClAg	11, 63	Distorted RS, KOH		high pressure	[31]
HCr	186	Wurtzite	H interstitial in metal, theoretical		[32]
TeSr	221	CsCl		high pressure	[27]
SMn	216, 186, 221	CsCl, Wurtzite	high pressure, alloying		[33–35]
SmTe	221	CsCl		high pressure	[36, 37]
NpAs	221	CsCl		high pressure	[38, 39]
PbSe	42, 221, 62, 63	CsCl, Distorted RS		high pressure	[40–43]
TePr	221	CsCl		high pressure	[36]
SnTe	216, 221	CsCl		high pressure	[44–46]
BrCs	221	CsCl		high pressure	[9, 19]
BaTe	221	CsCl		high pressure	[47, 48]
SeBa	221	CsCl		high pressure	[49, 50]
KN	129			mislabeled	[51, 52]
OBa	129, 194	NiAs		high pressure	[53–55]
ThAs	221	CsCl		high pressure	[39, 56]
NdSb	123	CsCl		high pressure	[4, 57]
TbSe	186	Wurtzite	thin film		[58, 59]
SmSe	186	Wurtzite	thin film		[59, 60]
PrAs	123	CsCl		high pressure	[61, 62]
SSr	221	CsCl		high pressure	[63, 64]
BrRb	221	CsCl		high pressure	[10, 65]
NAg	64			mislabeled	[66, 67]
PuAs	221	CsCl		high pressure	[68, 69]
PCe	221	CsCl		high pressure	[70, 71]
LaN	129	CsCl		high pressure	[72, 73]
HCs	221	CsCl		high pressure	[74, 75]
TeIn	140, 221	CsCl		high pressure	[76, 77]
DySe	186	Wurtzite	alloyed thin film		[59, 78]
LaS	64, 129	CsCl	misfit layered compound, high pressure		[79–81]
SnSb	216, 221	CsCl		high pressure	[44, 82, 83]
ClNa	221	CsCl		high pressure	[84, 85]
SPb	5, 39, 12, 221, 62, 63	CsCl, Distorted RS		high pressure	[13, 41, 86–91]
EuTe	221	CsCl		high pressure	[36]
LaSe	12		misfit layered compound		[81, 92]
SmS	139	Distorted RS		misfit layered compound	[93]
NpTe	221	CsCl		high pressure	[7, 94]
MnO	186	Wurtzite	thin film		[95]
AsU	221	CsCl		high pressure	[39, 96]
NPr	129	CsCl		high pressure	[97, 98]
CaO	64		composite crystal		[99, 100]
LaSb	123	CsCl		high pressure	[5, 6]
FCs	221	CsCl		high pressure	[9, 10]
BrAg	11	KOH		high pressure	[31]
KI	221	CsCl		high pressure	[101, 102]
BrTl	221, 63	CsCl, Distorted RS		high pressure	[19, 103, 104]
NdAs	123	CsCl		high pressure	[61, 105]
ClCs	221	CsCl		high pressure	[106, 107]
FRb	221	CsCl		high pressure	[102, 108]
PuTe	221	CsCl		high pressure	[7, 109]

SmAs	123	CsCl	high pressure	[61, 110]
NpSb	123	CsCl	high pressure	[7, 111]
KBr	221	CsCl	high pressure	[112, 113]
ClRb	221	CsCl	high pressure	[10, 114]
ThSe	221	CsCl	high pressure	[115, 116]
ICs	221, 62	CsCl, Distorted RS	high pressure	[9, 19, 117]
BiCe	123, 221	CsCl	high pressure	[118, 119]
FK	221	CsCl	high pressure	[10, 120]
ThSb	221	CsCl	high pressure	[56]
EuS	139	Distorted RS	misfit layered compound	[121, 122]

TABLE I: All compounds in the Materials Project Database with a rock-salt ground state and an experimentally reported polymorph. Inspection of references shows that there are no metastable polymorphs.

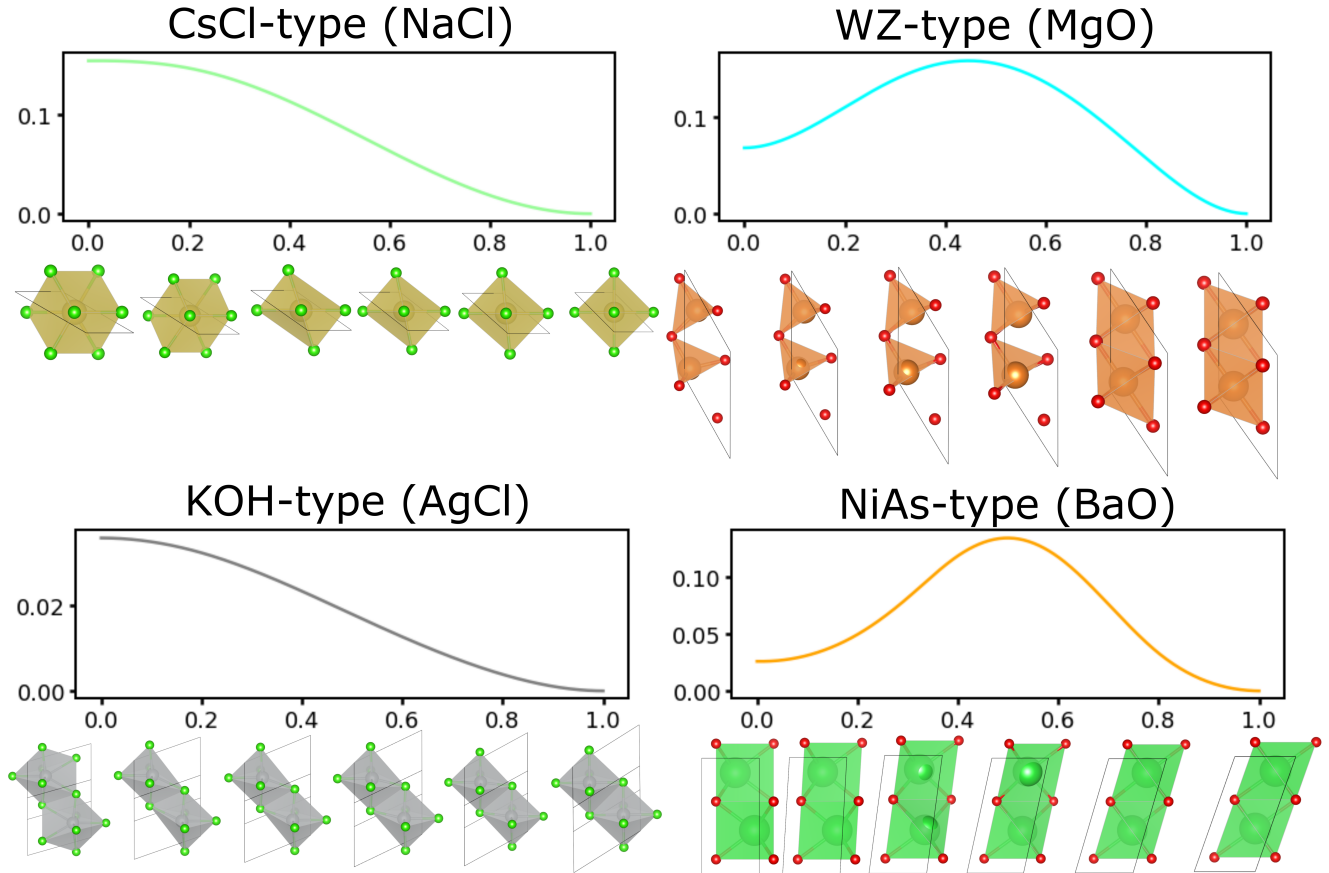


FIG. 5. Computed pathways and barriers for experimentally reported polymorphs of rocksalt compounds: CsCl-type in NaCl, NiAs-type in BaO, KOH-type in AgCl, and wurtzite-type in MgO.

space group number	frequency	ΔE_f (eV/atom)	NEB barrier (eV/atom)	description	name
225	1061	0	0	rocksalt (RS)	MgO_24_1960
194	42	0.035	0.057	hexagonal boron nitride (hBN)	MgO_24_1015
72	1	0.060		hBN with fault between rings	MgO_24_648
186	8	0.068	0.088	wurtzite (WZ)	MgO_24_1977
166	2	0.076	0.099	RS with stacking fault (face sharing octahedra)	MgO_24_1988
194	1	0.076	0.030	RS with stacking fault (face sharing octahedra)	MgO_24_345
14	1	0.078		hBN with fault	MgO_24_265
13	1	0.079		distorted trigonal bipyramids	MgO_24_202
160	26	0.081	0.101	rhombohedral WZ polytype	MgO_24_1296
140	1	0.082	0.001	trigonal bipyramids and octahedra with pores in the c-direction	MgO_24_141
36	3	0.087		buckled hBN	MgO_24_828
136	1	0.088	0.092	buckled hBN	MgO_24_607
160	1	0.098	0.053	face and edge sharing octahedra, trigonal prisms	MgO_24_1011
166	58	0.101	0.041	RS with stacking fault (face sharing octahedra)	MgO_24_266
12	1	0.102		RS with channels in c-direction	MgO_24_527
216	13	0.102	0.044	Zincblende (ZB)	MgO_24_775
12	1	0.105		distorted hBN	MgO_24_1806
36	1	0.113		buckled hBN	MgO_24_1699
187	8	0.130	0.30	face sharing octahedra and trigonal prisms	MgO_24_1220
12	1	0.130		RS with channels in c-direction	MgO_24_1971
194	13	0.150	0.062	RS stacking fault - all octahedra face sharing	MgO_24_728
36	21	0.155		square pyramids	MgO_24_1080
12	1	0.161		see-saws and tetrahedra with channels	MgO_24_1181
36	1	0.164		square pyramids	MgO_24_1817
38	1	0.168		square pyramids and tetrahedra	MgO_24_1246
161	1	0.218	0.009	disordered 7-fold coordination	MgO_24_1609
43	4	0.220		disordered 5-, 6-, and 7-fold	MgO_24_304
15	2	0.221		disordered see-saw, tetrahedra, square pyramids	MgO_24_937
194	1	0.244	0.019	nickelene (NC)	MgO_24_1249

TABLE II. Random sampling structures identified for MgO

space group number	frequency	ΔE_f (eV/atom)	NEB barrier (eV/atom)	description	name
225	45	0	0	rocksalt (RS)	C1Ta1_24_18
166	4	0.066	0.89	trigonal prisms and octahedra	C1Ta1_24_990
160	10	0.072	0.127	trigonal prisms and octahedra	C1Ta1_24_849
187	2	0.092	0.067	trigonal prisms and octahedra	C1Ta1_24_719
194	2	0.123	0.127	nickelene (NC)	C1Ta1_24_770
166	1	0.158	0.0636	RS with stacking fault	C1Ta1_24_909
63	1	0.206		distorted hBN	C1Ta1_24_451
12	1	0.216		layered trigonal prisms, distorted trigonal bipyramids, octahedra	C1Ta1_24_345
44	1	0.244		trigonal prisms and octahedra	C1Ta1_24_416
12	1	0.264		distorted trigonal prisms and 7-fold coordination	C1Ta1_24_581

TABLE III. Random sampling structures identified for TaC

space group number	frequency	ΔE_f (eV/atom)	NEB barrier (eV/atom)	description	name
225	84	0		rocksalt (RS)	PbTe_24_761
12	2	0.051		RS with channels in c-direction	PbTe_24_46
186	1	0.078	0.028	layered face-sharing octahedra	PbTe_24_1279
160	2	0.084	0.007	layered trigonal prisms and octahedra	PbTe_24_1527
12	1	0.108		disordered octahedra and square pyramids	PbTe_24_1532
12	1	0.117		disordered octahedra and square pyramids	PbTe_24_1716
38	1	0.131		RS with site swap	PbTe_24_417
38	1	0.174		RS with site swap	PbTe_24_1226

TABLE IV. Random sampling structures identified for PbTe

space group number	frequency	ΔE_f (eV/atom)	NEB barrier (eV/atom)	description	name
216	36	0	0	zincblende (ZB)	SiC_12_1523
160	4	0	0.237	tetrahedral rhombohedral WZ polytype	SiC_12_723
186	25	0.002	0.345	wurtzite (WZ)	SiC_12_1769
36	2	0.065		disordered tetrahedra	SiC_12_949
36	1	0.131		disordered tetrahedra	SiC_12_743
44	1	0.190		tetrahedra mixed with C-C and Si-Si bonds	SiC_12_1296
15	3	0.324		tetrahedra mixed with trigonal planar SiC_3	SiC_12_1149
12	1	0.364		disordered tetrahedra, C-C bonds	SiC_12_1882
152	1	0.366		disordered tetrahedra	SiC_12_690
20	1	0.403		disordered tetrahedra, C-C and Si-Si bonds	SiC_12_1245
12	1	0.481		disordered tetrahedra, C-C and Si-Si bonds	SiC_12_885
38	1	0.497		edge-sharing tetrahedra	SiC_12_128
25	1	0.524		disordered tetrahedra, C-C and Si-Si bonds	SiC_12_61
44	1	0.566		disordered tetrahedra, trigonal planar SiC_3 , C-C and Si-Si bonds	SiC_12_1859
43	1	0.566		disordered, distorted tetrahedra	SiC_12_364
107	1	0.709		5-fold, intermediate between ZB and RS	SiC_12_1932
225	2	0.740	0.001	rocksalt (RS)	SiC_12_6

TABLE V. Random sampling structures identified for SiC

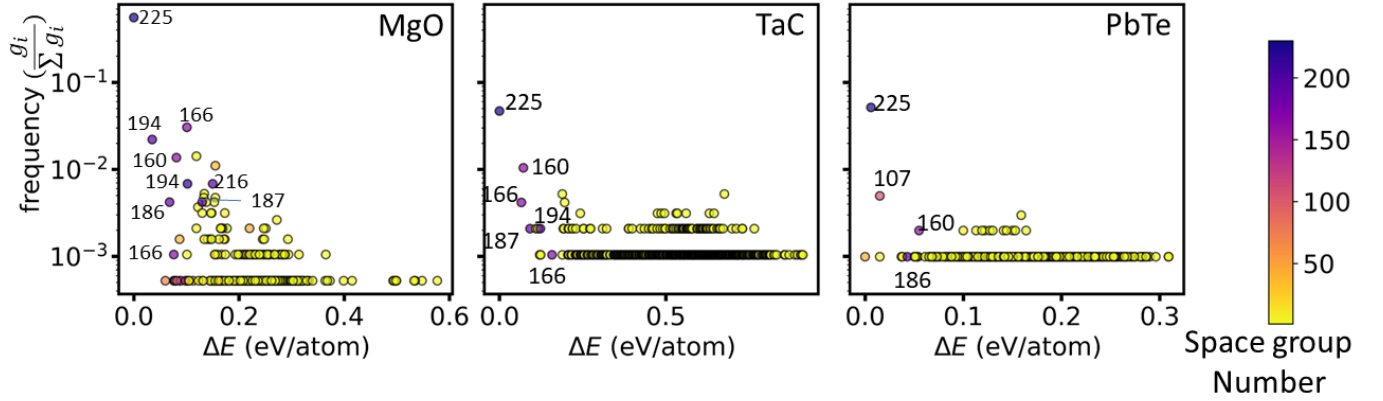


FIG. 6. The frequency of occurrence vs energy for each of MgO, TaC, and PbTe.

compound	polymorph	space group	structure types	realization condition	citations
MoN	191		layered material	space group misassigned	[123]
MoN	74		1-D chains	space group misassigned	[124, 125]
NbN	194		Face sharing octahedra	degenerate energy	[126]
SnSe	129		tetragonal layers	misfit layered compound	[127]
SnSe	63		1-D chains	space group misassigned	[41]
SnSe	59		2-D ribbons	space group misassigned	[41]
SnS	216		zincblende	Evaporation (citation only)	[128]
SnS	39		layered material	misfit layered compound	[129]
SnS	39		layered material	misfit layered compound	[130]
SnS	2		layered material	misfit layered compound	[131]
CdTe	63		distorted RS	high pressure	[132]
CdTe	63		distorted RS	high pressure	[132]
GeTe	62		Pnma layered	citation only	[133]
GeTe	60		buckled square ribbons	high pressure	[134]
LiI	194		face sharing octahedra	degenerate	[135]
TaN	191		close packed planes with trigonal prisms between	space group misassigned	[136]
TaN	191		close packed planes with octahedra between	space group misassigned	[137]
AgI	11		distorted rocksalt	high pressure	[31]
AgI	221		CsCl-type	high pressure	[138]
HgTe	63		distorted rocksalt	high pressure	[139]
BiSe	12			misfit layered compound	[140]
BiSe	12			misfit layered compound	[140]
BiSe	14			nonstoichiometric	[141]
MnTe	62		distorted NiAs	high pressure	[142]
InSb	59		distorted Rocksalt	high pressure	[143]
InSb	196		high pressure cadmium telluride	high pressure	[143]
InSb	221		CsCl-type	high pressure	[144]

TABLE VI. All compounds in the Materials Project Database with rocksalt reported as a polymorph. Inspection of references shows that there are no metastable polymorphs with energy above that of rocksalt.

compound	polymorph	space groups	structure types	realization condition	citations
Mg ₂ Sn	227, 194		Laves, cotunnite, hexagonal	high pressure, high temperature	[145, 146]
K ₂ S	194			mislabeled (refers to K ₂ SO ₄ compound)	[147]
Rb ₂ Te	227, 194		cotunnite, Ni ₂ In	high pressure, high temperature	[148]
Mg ₂ Pb	62			alloying	[149]
Mg ₂ Si	227, 194		cotunnite, hexagonal	high pressure, high temperature	[146]
Cs ₂ Se	62, 43		cotunnite, distorted fluorite	cotunnite degenerate, high pressure	[150]
CdF ₂	227		cotunnite	high pressure (reversible)	[151]
Rh ₂ As	62		cotunnite	high temperature	[152]
Mg ₂ Ge	227		Cubic Laves phase	high pressure	[153]
Li ₂ S	62		anticotunnite	high pressure (reversible)	[154]
ThO ₂	62		cotunnite	high pressure (reversible, sluggish)	[155]
CaF ₂	62		cotunnite	high pressure (partially reverts)	[156, 157]
SrF ₂	62, 194		cotunnite, Ni ₂ In	high pressure (partially reverts)	[158]
Rb ₂ S	62, 194		anticotunnite, Ni ₂ In	high pressure	[159]
Na ₂ S	62, 194		anticotunnite, Ni ₂ In	high pressure (reversible)	[160]
Ba ₂ F	62, 194		cotunnite, Ni ₂ In	high pressure (partially reverts)	[161]
Ba ₂ Cl	62		cotunnite, hydrated structure	high temperature (reversible), hydration	[162, 163]
PbF ₂	62		cotunnite	approximately degenerate	[164]

TABLE VII. All compounds in the Materials Project Database with a fluorite ground state and an experimentally reported polymorph. Inspection of references shows that while cotunnite is reported to be metastable for some chemistries, in those cases transformation back to fluorite is at least partially observed at room temperature.

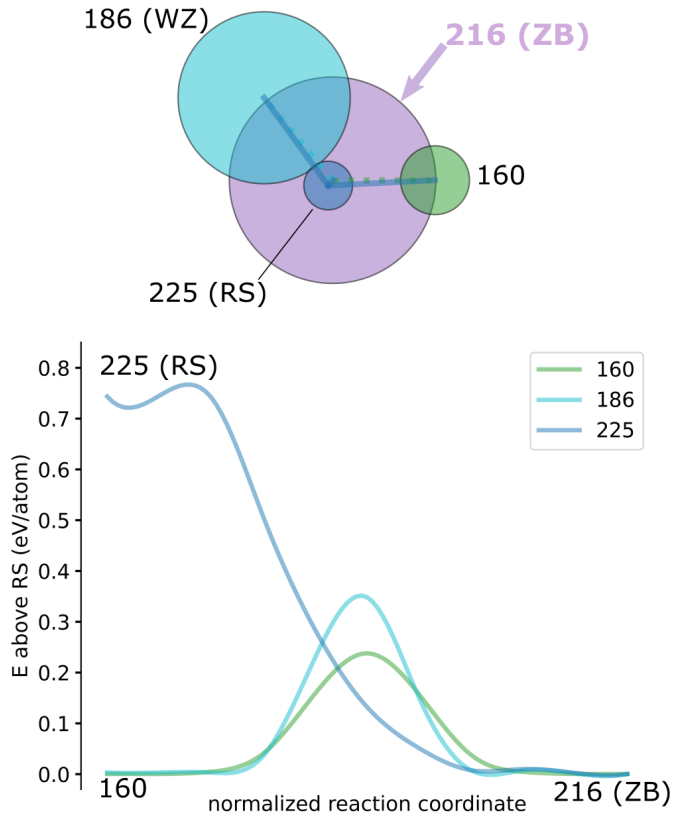


FIG. 7. A polymorph network representing the polymorphism of SiC. Zincblende is taken to be the origin. All other structures are labeled according to their space group number. The size of each node represents the frequency of occurrence of a structure in the random sample. Note that a fixed size is used to represent the width of the zincblende local minimum, and other points are scaled relative to this size. Structures are arranged so that the energy increases with the polar angle and the distance of each node from the zincblende center is proportional to the distance travelled by the atoms during phase transformation of that structure to zincblende. Dashed lines represent slow transformations from wurtzite and rhombohedral to zincblende. Solid lines represent fast transformations between rocksalt and the tetrahedral polymorphs.

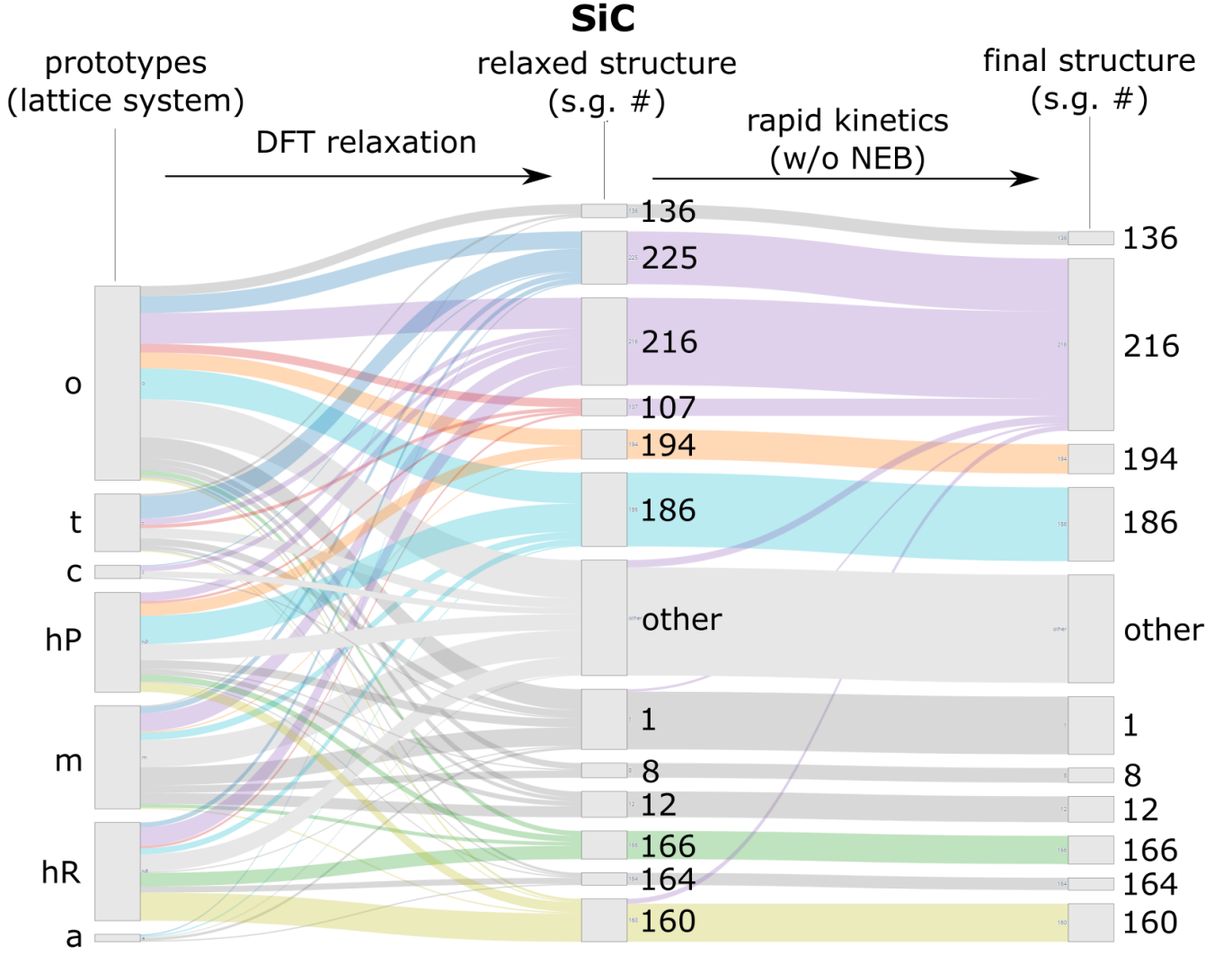


FIG. 8. Sankey diagrams showing the kinetic flow of 457 prototype structures found in the ICSD spanning the A_1B_1 chemical space for SiC. The bars on the left represent the distribution of the A_1B_1 prototypes across 7 crystal systems. Bars in the center display the distribution of space groups that these prototypes relax into. Structures which link to the s.g. #216 bar at the right end have kinetic barriers for transformation to zinblende less than 150 meV/atom. For this diagram, we assume that all structures with energy greater than the energy of rocksalt will transform quickly to rocksalt, and will therefore transform quickly to the zinblende ground state. Even under this condition, many fewer structures transform to the zinblende ground state in SiC than those that transform quickly to rocksalt in each of the figures in main body.

ICSD label	polymorph	space groups	name	energy (eV/atom)
091736		14	Cristobalite	-7.908
647410		154	Quartz low	-7.887
190370		136	Stishovite	-7.730
075486		92	Cristobalite low - alpha	-7.904
067121		152	Quartz low	-7.897
077459		227	Cristobalite beta high	-7.905
040900		20	Tridymite	-7.909
089277		154	Quartz low	-7.899
089289		180	Quartz high	-7.899
056473		4	Tridymite	-7.909
162660		122	Cristobalite beta	-7.909
172295		15	Coesite	-7.869
094091		19	Tridymite	-7.908
030795		40	Tridymite O	-7.910
162616		198	Cristobalite beta	-7.905
200478		194	Tridymite 2H high (Gibbs Model)	-7.906
162618		122	Cristobalite beta	-7.910
040137		15		-7.902
029343		182	Tridymite 2H low (subcell)	-7.907
192626		58	Ferrierite, siliceous	-7.900
056320		227	Dodecasil 3C	-7.902
067669		15	Moganite	-7.899
064980			Quartz high	-6.860
085586		166	Chabazite	-7.897
048153		191	Dodecasil 1H	-7.905
048154		227	Dodecasil 3C	-7.902
183701		229	Sodalite	-7.904
065497		71		-7.900
093975		181	Quartz high	-7.899
		225	Fluorite	-6.661
			Glass ensemble	-7.529

TABLE VIII. Energies of named polymorphs of SiO₂. All polymorphs have energy below that of SiO₂ in the fluorite structure.

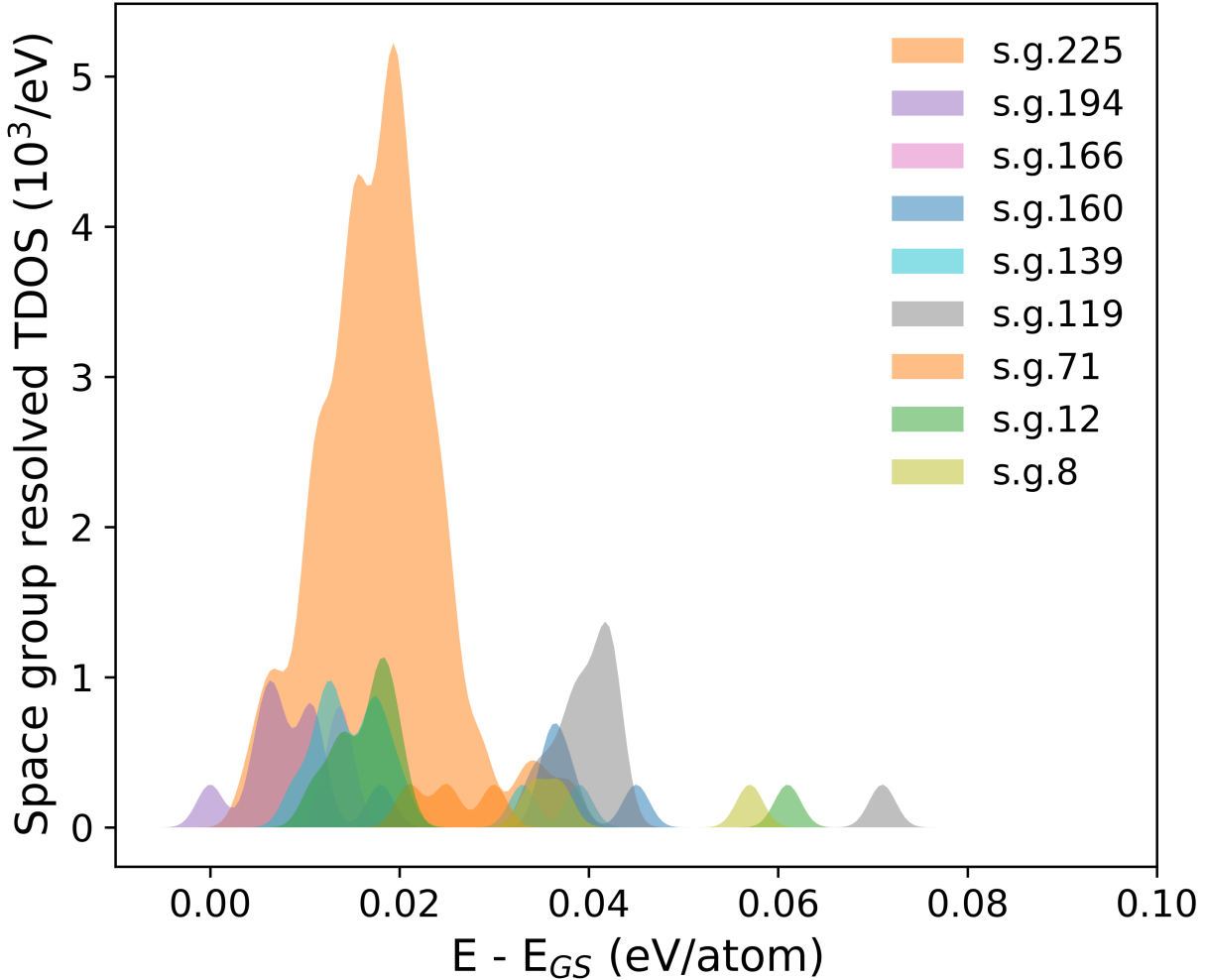


FIG. 9. The thermodynamic density of states for a hypothetical compound MgZnCuO₃. Despite the fact that both Zn and Cu prefer 4-fold coordination in oxides, rocksalt is by far the most abundant structure in random sampling of this compound. This displays the statistical relevance of the rocksalt structure for high-entropy systems.

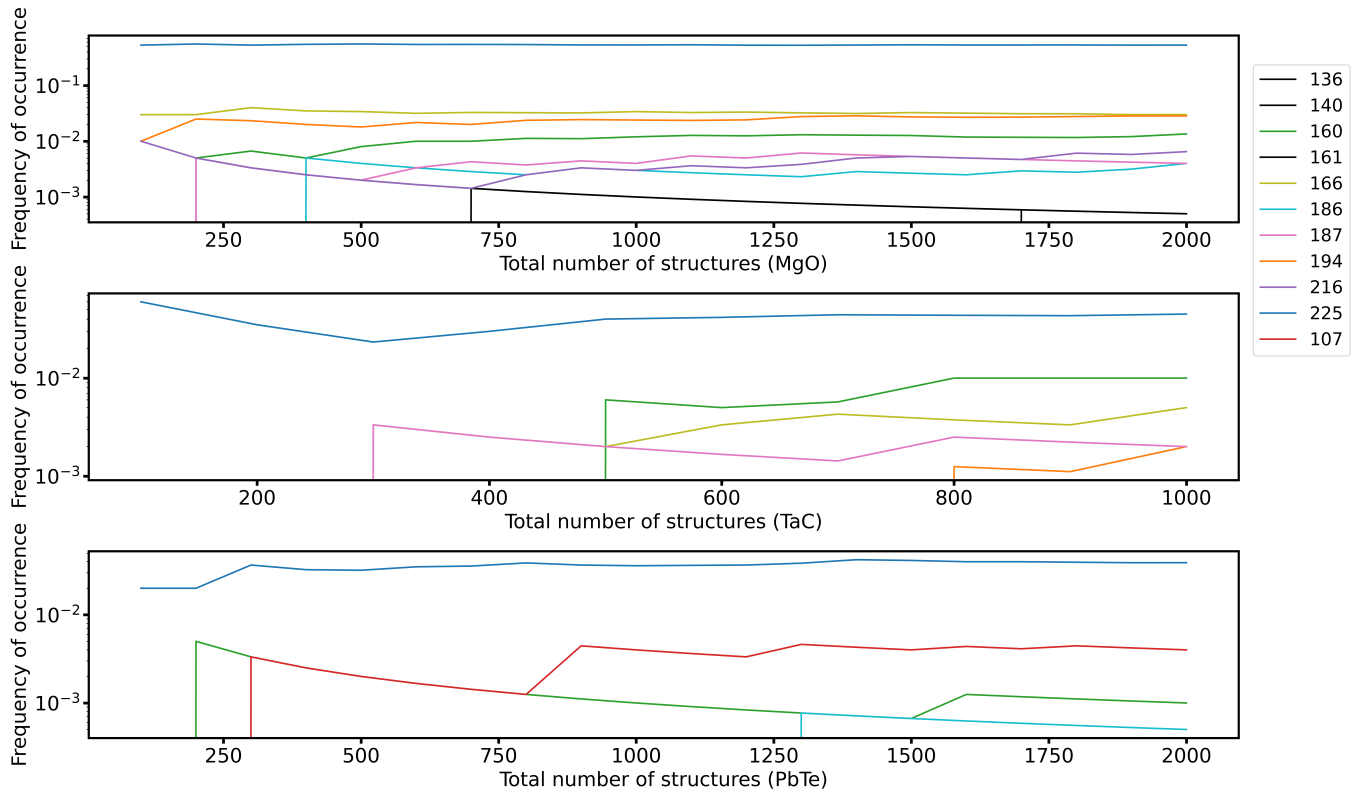


FIG. 10. Convergence of the high symmetry structures with respect to total number of structures for random sampling on each of MgO, TaC, and PbTe.

[1] H. Swanson and W. Davey, National Bureau of Standards (U.S.), Circular **539**, 31 (1955).

[2] L. Kirkpatrick and R. Dickinson, Journal of the American Chemical Society **49**, 2327 (1927).

[3] G. Samsonov, M. Abdusalyanova, and K. Shokirov, Inorganic Materials **10**, 790 (1974).

[4] J. Hayashi, I. Shirotani, Y. Tanaka, T. Adachi, O. Shimomura, and T. Kikegawa, Solid State Communications **114**, 561 (2000).

[5] P. Holbourn and F. Woodhams, Journal of Solid State Chemistry **39**, 186 (1981).

[6] J. Leger, D. Ravot, and J. Rossat Mignod, Journal of Physics C **17**, 4935 (1984).

[7] S. Dabos-Seignon, U. Benedict, S. Heathman, J. Spirlet, and M. Pages, Journal of the Less-Common Metals **160**, 35 (1990).

[8] C. Makode, J. Pataiya, M. Aynyas, and S. P. Sanyal, AIP Conference Proceedings **1536**, 925 (2013).

[9] E. Posnjak and R. Wyckoff, Journal of the Washington Academy of Sciences **12**, 248 (1922).

[10] C. Weir and G. Piermarini, Journal of Research of the National Bureau of Standards, Section A. Physics and Chemistry **68**, 105 (1964).

[11] G. Ugur, S. Ugur, A. Erkisi, and F. Soyalp, Int. J. Mod. Phys. **22**, 5027 (2008).

[12] I. Shirotani, K. Yamanashi, J. Hayashi, N. Ishimatsu, O. Shimomura, and T. Kikegawa, Solid State Communications **127**, 573 (2003).

[13] S. Kabalkina, N. Serebryanova, and L. Vereshchagin, Soviet Physics - Solid State (New York) **10**, 574 (1968).

[14] Y. Li, C. Lin, H. Li, X. Li, and J. Liu, High pressure research **33**, 713 (2013).

[15] R. J. Korkosz, T. C. Chasapis, S.-h. Lo, J. W. Doak, Y. J. Kim, C.-I. Wu, E. Hatzikraniotis, T. P. Hogan, D. N. Seidman, C. Wolverton, V. P. Dravid, and M. G. Kanatzidis, Journal of the American Chemical Society **136**, 3225 (2014).

[16] Y. Fujii, K. Kitamura, A. Onodera, and Y. Yamada, Solid State Communications **49**, 135 (1984).

[17] D. Walker, P. Verma, L. Cranswick, R. Jones, S. Clark, and S. Buhre, American Mineralogist **89**, 204 (2004).

[18] L. Shamovskii and A. Shushkanov, Doklady Akademii Nauk SSSR **181**, 862 (1968).

[19] M. Blackman and I. Khan, Proceedings of the Physical Society, London **77**, 471 (1961).

[20] D. Becker and H. Beck, Zeitschrift fuer Kristallographie (1979-2010) **219**, 348 (2004).

[21] R. Penneman and E. Staritzky, Journal of Inorganic and Nuclear Chemistry **6**, 112 (1958).

[22] M. Strada, Gazzetta Chimica Italiana **64**, 400 (1934).

[23] H. Wilhelm and P. Chiotti, Transactions of the American Society for Metals **42**, 1295 (1950).

[24] R. Johnsen and P. Norby, Journal of Physical Chemistry C **113**, 19061 (2009).

[25] V. Tsirel'son, A. Avilov, Y. Abramov, E. Belokoneva, R. Kitaneh, and D. Feil, Acta Crystallographica, Section B: Structural Science **54**, 8 (1998).

[26] M. Zwijnenburg and S. Bromley, Physical Review, Serie 3. B - Condensed Matter (18,1978-) **83**, 024104 (2011).

[27] H. Zimmer, H. Winzen, and K. Syassen, Physical Review, Serie 3. B - Condensed Matter (18,1978-) **32**, 4066 (1985).

[28] C. Sifi, M. Slimani, and H. Meradji, Materials Science and Engineering, IOP conference series **28**, 012031 (2012).

[29] J. Ungelenk, Naturwissenschaften **49**, 252 (1962).

[30] A. Roberts, K. Venance, T. Seward, J. Grice, and W. Paar, Mineralogical Record **37**, 165 (2006).

[31] S. Hull and D. Keen, Physical Review, Serie 3. B - Condensed Matter (18,1978-) **59**, 750 (1999).

[32] C. Snavely and D. Vaughan, Journal of the American Chemical Society **71**, 313 (1949).

[33] L. Corliss, N. Elliott, and J. Hastings, Physical Review (1,1893-132,1963/141,1966-188,1969) **104**, 924 (1956).

[34] H. Wiedemeier and A. Gary Sigai, High Temperature Science **1**, 18 (1969).

[35] F. Mehmed and H. Haraldsen, Zeitschrift fuer Anorganische und Allgemeine Chemie (1950) (DE) **235**, 193 (1938).

[36] A. Chatterjee, A. Singh, and A. Jayaraman, Physical Review, Serie 3. B - Solid State (1,1970-17,1977) **6**, 2285 (1972).

[37] E. Yarembash, E. Tyurin, A. Reshchikova, A. Karabekov, and N. Klinava, Inorganic Materials **7**, 661 (1971).

[38] S. Langridge, W. Stirling, G. Lander, J. Rebizant, J. Spirlet, D. Gibbs, and O. Vogt, Europhysics Letters **25**, 137 (1994).

[39] S. Dabos, C. Dufour, U. Benedict, J. Spirlet, and M. Pages, Physica B and C (Netherland) (79,1975-) **144**, 79 (1986).

[40] S. Wang, C. Zang, Y. Wang, L. Wang, J. Zhang, C. Childs, H. Ge, H. Xu, H. Chen, D. He, and Y. Zhao, Inorganic Chemistry **54**, 4981 (2015).

[41] T. Chattopadhyay, H. von Schnerring, W. Grosshans, and W. Holzapfel, Physica B and C (Netherland) (79,1975-) **139**, 356 (1986).

[42] A. Mariano and K. Chopra, Applied Physics Letters **10**, 282 (1967).

[43] C. Auriel, R. Roesky, A. Meerschaut, and J. Rouxel, Materials Research Bulletin **28**, 247 (1993).

[44] V. Goldschmidt, Skrifter utgitt av det Norske Videnskaps-Akademii i Oslo 1: Matematisk-Naturvidenskapelig Klasse **1927**, 1 (1927).

[45] A. Onodera, Y. Fujii, and S. Sugai, Physica B and C (Netherland) (79,1975-) **139**, 240 (1986).

[46] E. Rogacheva, G. Gorne, S. Laptev, A. Arinkin, and T. Vesiene, Izvestiya Akademii Nauk SSSR, Neorganicheskie Materialy **22**, 41 (1986).

[47] T. Grzybowski and A. Ruoff, Materials Research Society Symposia Proceedings **22**, 43 (1984).

[48] T. Grzybowski and A. Ruoff, Physical Review, Serie 3. B - Solid State (1,1970-17,1977) **3**, 755 (1971).

[49] Y. Lyskova and A. Vakhobov, Inorganic Materials **11**, 1784 (1975).

[50] T. Grzybowski and A. Ruoff, Physical Review, Serie 3. B - Condensed Matter (18,1978-) **27**, 6502 (1983).

[51] R. Juza and H. Liedtke, Zeitschrift fuer Anorganische und Allgemeine Chemie (1950) (DE) **290**, 204 (1957).

[52] M. Nagib, E. von Osten, and H. Jacobs, Atomkernenergie **29**, 41 (1977).

[53] L. Lingun, Journal of Applied Physics **42**, 3702 (1971).

[54] D. Taylor, Transactions and Journal of the British Ceramic Society **83**, 5 (1984).

[55] S. Weir, Y. Vohra, and A. Ruoff, Physical Review, Serie 3. B - Condensed Matter (18,1978-) **33**, 4221 (1986).

[56] L. Gerward, J. Olsen, U. Benedict, S. Dabos, H. Luo, J. Itie, and O. Vogt, High Temperatures-High Pressures **20**, 545 (1988).

[57] P. Manfrinetti, A. Provino, A. Morozkin, and O. Isnard, Journal of Alloys and Compounds **487**, L28 (2009).

[58] A. Eliseev, I. Orlova, L. Martynova, A. Pechennikov, and V. Chechernikov, Inorganic Materials **23**, 1833 (1987).

[59] A. Singh and O. Srivastava, Zeitschrift fuer Metallkunde **68**, 768 (1977).

[60] J. Miller, L. Matson, and R. Himes, Proceedings of the Conference of Rare Earth Research, 2nd, Colorado **1962**, 233 (1962).

[61] I. Shirotani, K. Yamanashi, J. Hayashi, Y. Tanaka, N. Ishimatsu, O. Shimomura, and T. Kikegawa, Journal of Physics: Condensed Matter **13**, 1939 (2001).

[62] A. Iandelli and E. Botti, Atti della Accademia Nazionale dei Lincei, Classe di Scienze Fisiche, Matematiche e Naturali, Rendiconti, Serie 7 (1, 1925-1945) **25**, 498 (1937).

[63] J. Flahaut, L. Domange, and M. Patrie, Bulletin de la Societe Chimique de France (Vol=Year) **1962**, 2048 (1962).

[64] S. Ugur, Materials Science and Engineering B: Solid-state Materials for Advanced Technology **162**, 116 (2009).

[65] P. Cortona, Physical Review, Serie 3. B - Condensed Matter (18,1978-) **46**, 2008 (1992).

[66] W. Chen and J.-Z. Jiang, Journal of Alloys and Compounds **499**, 243 (2010).

[67] A. Niggli, Zeitschrift fuer Kristallographie, Kristallgeometrie, Kristallphysik, Kristallchemie (-144,1977) **111**, 269 (1959).

[68] S. Dabos-Seignon, U. Benedict, J. Spirlet, and M. Pages, Journal of the Less-Common Metals **153**, 133 (1989).

[69] J. Charvillat and D. Damien, Inorganic and Nuclear Chemistry Letters **9**, 559 (1973).

[70] I. Vedel, A. Redon, J. Rossat Mignod, O. Vogt, and J. Leger, Journal of Physics C **20**, 3439 (1987).

[71] S. Ono, K. Nomura, and H. Hayakawa, Journal of the Less-Common Metals **38**, 119 (1974).

[72] S. B. Schneider, D. Baumann, A. Salamat, and W. Schnick, Journal of Applied Physics **111**, 093503 (2012).

[73] G. L. Olcese, Journal of Physics F **9**, 569 (1979).

[74] E. Pomyatovskii and I. Bashkin, Zeitschrift fuer Physikalische Chemie (Frankfurt Am Main) **146**, 137 (1985).

[75] E. Zintl and A. Harder, Zeitschrift fuer Physikalische Chemie, Abteilung B: Chemie der Elementarprozesse, Aufbau der Materie **14**, 265 (1931).

[76] F. Faita, C. Campos, K. Ersching, and P. Pizani, Materials Chemistry and Physics **125**, 257 (2011).

[77] T. Chattopadhyay, R. Santandrea, and H. von Schnerring, Journal of Physics and Chemistry of Solids **46**, 351 (1985).

[78] G. Olcese, Atti della Accademia Nazionale dei Lincei, Classe di Fisiche, Matematiche e Naturali, Rendiconti **31**, 256 (1961).

[79] K. Friese, O. Jarchow, and K. Kato, Zeitschrift fuer Kristallographie (1979-2010) **212**, 648 (1997).

[80] J. de Boer, A. Meetsma, T. Zeinstra, R. Haange, and G. Wiegers, Acta Crystallographica, Section C: Crystal Structure Communications **47**, 924 (1991).

[81] Z. Charifi, H. Baaziz, Y. Saeed, A. Hussain Reshak, and F. Soltani, Physica Status Solidi B - Basic Solid State Physics **249**, 18 (2012).

[82] T. Kolobyanina, S. Kabalkina, L. Vereshchagin, M. Kachan, and V. Losev, High Temperatures-High Pressures **4**, 207 (1972).

[83] V. Losev, S. Kabalkina, and L. Vereshchagin, Soviet Physics - Solid State (New York) **12**, 2374 (1970).

[84] S. Abrahams and J. Bernstein, Acta Crystallographica (1,1948-23,1967) **18**, 926 (1965).

[85] W. Zhang, A. R. Oganov, A. F. Goncharov, Q. Zhu, S. E. Boulfelfel, A. O. Lyakhov, E. Stavrou, M. Somayazulu, V. B. Prakapenka, and Z. Konopkova, Science **342**, 1502 (2013).

[86] M. Onoda, K. Kato, Y. Gotoh, and Y. Oosawa, Acta Crystallographica, Section B: Structural Science **46**, 487 (1990).

[87] G. Wiegers, A. Meetsma, R. Haange, S. van Smaalen, J. de Boer, A. Meerschaut, P. Rabu, and J. Rouxel, Acta Crystallographica, Section B: Structural Science **46**, 324 (1990).

[88] I. Meerschaut, C. Auriel, and J. Rouxel, Journal of Alloys and Compounds **183**, 129 (1992).

[89] R. Sakthi Sudar Saravanan, M. Meena, P. D., and C. Mahadevan, Journal of Alloys and Compounds **627**, 69 (2015).

[90] D. Zagorac, K. Doll, J. Schoen, and M. Jansen, Physical Review, Serie 3. B - Condensed Matter (18,1978-) **84**, 045206 (2011).

[91] S. van Smaalen, A. Meetsma, G. Wiegers, and J. de Boer, Acta Crystallographica, Section B: Structural Science **47**, 314 (1991).

[92] Y. Ren, A. Meetsma, A. Spijkerman, and G. Wiegers, Zeitschrift fuer Kristallographie (1979-2010) **212**, 586 (1997).

[93] A. Meerschaut, C. Auriel, A. Lafond, C. Deudon, P. Gressier, and J. Rouxel, European Journal of Solid State Inorganic Chemistry **28**, 581 (1991).

[94] F. Wastin, J. Spirlet, and J. Rebizant, Journal of Alloys and Compounds **219**, 232 (1995).

[95] N. K. Min, K. Yong-Il, J. Younghun, L. S. Mi, K. B. G., C. Ran, C. Sang-Il, S. Hyunjoon, and P. J. T., Journal of the American Chemical Society **134**, 8392 (2012).

[96] W. Trzebiatowski, A. Sepichowska, and A. Zygmunt, Bulletin de l'Academie Polonaise des Sciences, Serie des Sciences Chimiques **12**, 687 (1964).

[97] P. Ettmayer, J. Waldhart, and A. Vendl, Monatshefte fuer Chemie **110**, 1109 (1979).

[98] H. Cynn, M. Lipp, W. Evans, and Y. Ohishi, Journal of Physics: Conference Series **215**, 012010 (2010).

[99] M. Isobe, M. Onoda, M. Shizuya, M. Tanaka, and E. Takayama Muromachi, Journal of the Physical Society of Japan **76**, 014602 (2007).

[100] I. Oftedal, Zeitschrift fuer Physikalische Chemie (Leipzig) **128**, 154 (1927).

[101] L. Vegard, Zeitschrift fuer Physik **5**, 17 (1921).

[102] G. Piermarini and C. Weir, Journal of Research of the National Bureau of Standards, Section A. Physics and Chemistry **66**, 325 (1962).

[103] R. Singh, R. Singh, and M. Rajagopalan, Physica B,

Condensed Matter **406**, 1717 (2011).

[104] J. Ungelenk, Zeitschrift fuer Kristallographie (1979-2010) **219**, 348 (2004).

[105] J. Taylor, L. Calvert, J. Despault, E. Gabe, and J. Murray, Journal of the Less-Common Metals **37**, 217 (1974).

[106] C. West, Zeitschrift fuer Kristallographie, Kristallgeometrie, Kristallphysik, Kristallchemie (-144,1977) **88**, 94 (1934).

[107] H. Swanson and R. Fuyat, National Bureau of Standards (U.S.), Circular **539**, 44 (1953).

[108] V. Goldschmidt, Skrifter utgitt av det Norske Videnskaps-Akadem i Oslo 1: Matematisk-Naturvidenskapelig Klasse **1926**, 1 (1926).

[109] O. Kruger and J. Moser, Journal of Physics and Chemistry of Solids **28**, 2321 (1967).

[110] R. Beeken and J. Schweitzer, Physical Review, Serie 3. B - Condensed Matter (18,1978-) **23**, 3620 (1981).

[111] A. Mitchell and D. Lam, Journal of Nuclear Materials **39**, 219 (1971).

[112] A. Dewaele, A. Belonoshko, G. Garbarino, F. Occelli, P. Bouvier, M. Hanfland, and M. Mezouar, Physical Review, Serie 3. B - Condensed Matter (18,1978-) **85**, 214105 (2012).

[113] G. Finch and S. Fordham, Proceedings of the Physical Society, London **48**, 85 (1936).

[114] H. Ott, Zeitschrift fuer Kristallographie, Kristallgeometrie, Kristallphysik, Kristallchemie (-144,1977) **63**, 222 (1926).

[115] J. Olsen, L. Gerward, U. Benedict, H. Luo, and O. Vogt, High Temperatures-High Pressures **20**, 553 (1988).

[116] R. d'Eye, P. Sellman, and J. Murray, Journal of the Chemical Society **1952**, 2555 (1952).

[117] J. Beintema, Zeitschrift fuer Kristallographie, Kristallgeometrie, Kristallphysik, Kristallchemie (-144,1977) **97**, 300 (1937).

[118] W. Feng, H. Hu, X. Xiao, S. Cui, Z. Lv, G. Zhang, and C. Wu, Computational Materials Science, Elsevier **53**, 75 (2012).

[119] M. Abdusalyamova, O. Rakhmatov, and K. Shokirov, Russian Metallurgy **1988**, 183 (1988).

[120] A. Hull, Transactions of the American Institute for Electrical Engineers **38**, 1445 (1919).

[121] L. Cario, A. Meerschaut, C. Deudon, and J. Rouxel, C.R. Acad. Sci. Paris, T. 1, Serie II **1**, 269 (1998).

[122] A. Eliseev, O. Sadovskaya, and N. V. Tam, Izvestiya Akademii Nauk SSSR, Neorganicheskie Materialy **10**, 2134 (1974).

[123] N. Troitskaya and Z. Pinsker, Kristallografiya **6**, 43-48 (1961).

[124] Z. X. Dong and K. Range, Journal of Alloys and Compounds **296**, 72 (2000).

[125] Z.-X. Yang, X.-Y. Kuang, M.-M. Zhong, and X.-F. Huang, Solid State Sciences **28**, 20 (2014).

[126] N. Schoenberg, Acta Chemica Scandinavica (1-27,1973-42,1988) **8**, 208 (1954).

[127] G. Wiegers and W. Zhou, Materials Research Bulletin **26**, 879-885 (1991).

[128] S. Badachhapa and A. Goswami, Journal of the Physical Society of Japan Supplement B2 **17**, 251-253 (1962).

[129] L. Hoistad, A. Meerschaut, P. Bonneau, and J. Rouxel, Journal of Solid State Chemistry **114**, 435 (1995).

[130] A. Meetsma, G. Wiegers, R. Haange, and J. de Boer, Acta Crystallographica. Section A: Foundations of Crystallography **45**, 285 (1989).

[131] G. Wiegers and I. Meerschaut, Journal of Alloys and Compounds **178**, 351 (1992).

[132] R. Nelmes, M. McMahon, N. Wright, and D. Allan, Physical Review, Serie 3. B - Condensed Matter (18,1978-) **51**, 15724 (1995).

[133] S. Karbanov, V. Zlomanov, and A. Novoselova, Doklady Chemistry **182**, 862 (1968).

[134] A. Onodera, I. Sakamoto, Y. Fujii, N. Mori, and S. Sugai, Physical Review, Serie 3. B - Condensed Matter (18,1978-) **56**, 7935 (1997).

[135] H. Ott, Physikalische Zeitschrift **24**, 209 (1923).

[136] T. Chihi, M. Fatmi, and B. Ghebouli, Solid State Communications **151**, 1672 (2011).

[137] G. Brauer, E. Mohr, A. Neuhaus, and A. Skogan, Monatshefte fuer Chemie **103**, 794 (1972).

[138] L. Adams and B. Davis, Proceedings of the National Academy of Sciences, U.S.A. **48**, 982 (1962).

[139] H. Aimin, Y. X. Cui, Y. Ruomeng, G. C. Xiao, H. Yonghao, L. R. Ping, and T. Yongjun, Journal of Physics and Chemistry of Solids **70**, 433 (2009).

[140] S. M. Clarke and D. E. Freedman, Inorganic Chemistry **54**, 2765 (2015).

[141] B. Aurivillius, O. von Heidenstamm, and I. Jonsson, Acta Chemica Scandinavica (1-27,1973-42,1988) **14**, 944 (1960).

[142] M. Mimasaka, I. Sakamoto, K. Murata, J. Fujii, and A. Onodera, Journal of Physics C **20**, 4689 (1987).

[143] S.-C. Yu, I. Spain, and E. Skelton, Journal of Applied Physics **49**, 4741 (1978).

[144] C. Vanderborgh, Y. Vohra, and A. Ruoff, Physical Review, Serie 3. B - Condensed Matter (18,1978-) **40**, 12450 (1989).

[145] Y. Fei, S. J. Xun, and C. T. Hong, Physica B, Condensed Matter **406**, 1789 (2011).

[146] D. Boudemagh, D. Fruchart, R. Haettel, E. Hill, A. Lacoste, L. Ortega, N. Skryabina, J. Tobola, and P. Wolfers, Diffusion and Defect Data - Solid State Data B: Solid State Phenomena **170**, 253 (2011).

[147] H. Fischmeister, Monatshefte fuer Chemie **93**, 420 (1962).

[148] K. Stoewe, Zeitschrift fuer Kristallographie (1979-2010) **219**, 359 (2004).

[149] J. M. Eldridge, E. Miller, and K. Komarek, Transactions of the Metallurgical Society of Aime **233**, 1303 (1965).

[150] H. Sommer and R. Hoppe, Zeitschrift fuer Anorganische und Allgemeine Chemie (1950) (DE) **429**, 118 (1977).

[151] G. T. Liu, H. Wang, Y. M. Ma, and Y. M. Ma, Solid State Communications **151**, 1899 (2011).

[152] A. Kjekshus and K. Skaug, Acta Chemica Scandinavica (1-27,1973-42,1988) **26**, 2554 (1972).

[153] R. LaBotz, D. Mason, and D. O'Kane, Journal of the Electrochemical Society **110**, 127 (1963).

[154] A. Grzechnik, A. Vegas, K. Syassen, I. Loa, M. Hanfland, and M. Jansen, Journal of Solid State Chemistry **154**, 603 (2000).

[155] M. Idiri, T. Le Bihan, S. Heathman, and J. Rebizant, Physical Review, Serie 3. B - Condensed Matter (18,1978-) **70**, 014113 (2004).

[156] L. Gerward, J. Olsen, S. Streenstrup, M. Malinovskii, S. Asbrink, and A. Waskowska, Journal of Applied Crystallography **25**, 578 (1992).

[157] E. Morris, T. Groy, and K. Leinenweber, Journal of Physics and Chemistry of Solids **62**, 1117 (2001).

- [158] J. Wang, C. Ma, D. Zhou, Y. Xu, M. Zhang, W. Gao, H. Zhu, and Q. Cui, *Journal of Solid State Chemistry* **186**, 231 (2012).
- [159] D. Santamaria-Perez, A. Vegas, C. Muehle, and M. Jansen, *Acta Crystallographica, Section B: Structural Science* **67**, 109 (2011).
- [160] A. Vegas, A. Grztechnik, K. Syassen, I. Loa, M. Hanfland, and M. Jansen, *Acta Crystallographica, Section B: Structural Science* **57**, 151 (2001).
- [161] J. Leger, J. Haines, A. Atouf, O. Schulte, and S. Hull, Physical Review, Serie 3. B - Condensed Matter (18,1978-) **52**, 13247 (1995).
- [162] S. Hull, S. Norberg, I. Ahmed, S. Eriksson, and C. Mohn, *Journal of Solid State Chemistry* **184**, 2925 (2011).
- [163] A. Haase and G. Brauer, *Zeitschrift fuer Anorganische und Allgemeine Chemie* (1950) (DE) **441**, 181 (1978).
- [164] L. Ehm, K. Knorr, F. Maedler, H. Voigtlaender, E. Busetto, A. Cassetta, A. Lausi, and B. Winkler, *Journal of Physics and Chemistry of Solids* **64**, 919 (2003).